J. Fluid Mech. (1974), *vol.* 64, *part* 1, *pp.* 177–194
Printed in Great Britain

The formation of atmospheric fronts downstream in a deformation field

By BRIAN J. HOSKINS

Geophysical Fluid Dynamics Program, Princeton University, Princeton, New Jersey†

(Received 17 September 1973)

An analytical study is made of simple models of steady fronts in the atmosphere in which the temperature field is subjected to deformation as the fluid moves downstream in a large-scale horizontal flow. One fundamental approximation is made and then a Lagrangian method, in which fluid particles are identified by conservation of entropy and potential vorticity, and by Bernoulli's theorem, enables the steady problem to be solved. Solutions for models of surface fronts and upper tropospheric fronts are compared with those obtained from a model in which there is no variation along the front and the frontogenesis proceeds in time. If the thermal wind is comparable with the basic wind, and the potential vorticity is not negligible in some sense, the frontogenesis is increased where the thermal wind opposes the basic flow but decreased where it reinforces the flow.

1. Introduction

The idea of the atmospheric front has been an important weapon in the conceptual armoury of the synoptic meteorologist since its introduction by Bjerknes and the Norwegian school of meteorologists in 1919. They envisaged a sloping surface of discontinuity between the cold polar air and warmer air of temperate latitudes. On this surface disturbances develop and these are the familiar cyclones. With the advent of more upper-air observations and on the theoretical side the development of quasi-geostrophic theory, the emphasis shifted. Cyclones formed by baroclinic instability in a region of temperature gradient (Charney 1947; Eady 1949) became the fundamental entities. As a secondary phenomenon in these cyclones, fronts tend to form and dissipate. The deformation fields in which fronts form may also be associated with other phenomena such as orographically induced long waves. On some occasions, disturbances growing on fronts much as described by Bjerknes can be very important. Because of the rapid change in weather across atmospheric fronts, and the rainfall at them, their formation and structure is still of great interest.

In Hoskins (1971), Hoskins & Bretherton (1972) and Hoskins (1972), hereafter referred to as I, II and III, the author introduced simple models in which large-scale horizontal flow patterns perturb the temperature field and the

† Present address: U.K. Universities Atmospheric Modelling Group, University of Reading.

atmosphere responds in a nonlinear manner. One model, which we here refer to as the time deformation model, considers a temperature field independent of y compressed by the 'deformation field' $u = -\alpha x$, $v = \alpha y$. There are two basic kinds of atmospheric front. The surface front has very strong gradients near the surface of the earth, but these die away rapidly above the surface (Sanders 1955). The upper tropospheric front has large gradients in the upper troposphere which have been shown to be connected with the subsidence of upper tropospheric and stratospheric air (Reed & Danielsen 1959). The formation of the surface front was modelled by a time deformation model with an atmosphere of initially uniform static stability representing the troposphere. The upper tropospheric front model had two regions of static stability representing the troposphere and stratosphere. Comparison with observation suggested the realism of these fronts.

The fundamental approximation in I, II and III was that the wind along the front was in geostrophic balance with the pressure gradient across the front (see §§ 2.2 and 2.3). Kelvin's circulation theorem then suggested the use of a semi-Lagrangian co-ordinate in the cross-front direction. The models were solved using conservation of entropy and potential vorticity.

In this paper we consider the formation of fronts in deformation fields like the above field, but we now consider the *steady* problem in which this frontogenesis occurs *downstream*. The front itself is independent of time, but fluid particles experience frontogenesis as they move through the system. A third conserved quantity in addition to entropy and potential vorticity is provided by Bernoulli's theorem. Making the same fundamental approximation as in the time deformation model, the three Lagrangian tracers enable solutions to be found given initial conditions at one cross-section upstream. The numerical work is simplified by the introduction of the semi-Lagrangian co-ordinate used in the time deformation model. Solutions are obtained and comparisons made with those from the time deformation model. Detailed comparison of the latter solutions with observed fronts was made in I, in particular, and will not be repeated here.

The equations of motion are introduced in § 2. Various approximations based on the dominance of Coriolis over inertial effects and their relevance in the frontogenesis problem are discussed. When atmospheric motions change the temperature distribution, additional motions are induced. However, in § 3 we first consider the possible steady-state deformation fields and their advection of a passive scalar. The Lagrangian study of a general model of frontogenesis is performed in § 4. In § 5 this is specialized to a one-region model to discuss the formation of surface fronts. Consideration of a two-region model in § 6 allows investigation of upper tropospheric frontogenesis.

2. The basic equations

2.1. *The primitive equations*

When the horizontal scale of motion of a rotating atmosphere is much larger than the vertical scale, to a very good approximation the horizontal component

of the rotation and the vertical component of acceleration may be neglected. The use of the pressure p as the vertical co-ordinate then makes the form of the pressure force and continuity equation similar to that for an incompressible fluid. As was done in the previous studies, the vertical co-ordinate used here is a function of pressure:

$$z = [1-(p/p_0)^\kappa]\, c_p \theta_0/g,$$

where p_0 and θ_0 are standard surface pressures and temperatures, c_p = specific heat at constant pressure, $\kappa = R/c_p$ and R is the gas constant. The top of the atmosphere ($p = 0$) is $z = z_a = c_p\theta_0/g$. If the potential temperature θ is defined by the relation

$$\text{entropy} = c_p \ln\theta,$$

θ is conserved on a fluid particle in the absence of heat sources and sinks. It is related to the temperature T by

$$\theta = T(p_0/p)^\kappa.$$

A pseudo-density may also be defined:

$$r(z) = \rho_0(p/p_0)^{1-\kappa} = \rho_0[1-gz/c_p\theta_0]^{1/\kappa-1},$$

where ρ_0 is a standard surface density. Using the equation of state for a perfect gas, it is easily shown that increments in physical height $\mathfrak{z}$ are related to those in z by

$$\theta_0\, d\mathfrak{z} = \theta\, dz, \quad \rho\, d\mathfrak{z} = r\, dz.$$

For an adiabatic atmosphere ($\theta \equiv \theta_0$) $z = \mathfrak{z}$ and, quite generally, over much of the atmosphere z may be considered as approximately the physical height.

The inviscid adiabatic equations may be written as

$$\left.\begin{aligned} D\mathbf{u}/Dt + f\mathbf{k}\times\mathbf{u} + \nabla_2\phi = 0, \quad \phi_z = g\theta/\theta_0, \\ D\theta/Dt = 0, \quad \nabla.(r\mathbf{v}) = 0, \end{aligned}\right\} \tag{2.1}$$

where $w = Dz/Dt = -(Dp/Dt)/gr$, $\mathbf{k}$ = unit vertical vector,

$$\mathbf{u} = (u, v, 0), \quad \mathbf{v} = \mathbf{u} + w\mathbf{k},$$

$$\nabla_2 = (\partial/\partial x, \partial/\partial y, 0), \quad \nabla = \nabla_2 + \mathbf{k}\,\partial/\partial z,$$

$$D/Dt = \partial/\partial t + \mathbf{v}.\nabla, \quad \phi = \text{geopotential} = g\mathfrak{z},$$

f = Coriolis parameter = 2 × vertical component of rotation,

here taken as independent of position.

At $z = c_p\theta_0/g$, clearly we must have $w = 0$. At the surface of a smooth earth we should have $D\phi/Dt = 0$. But the surface pressure varies only within about 5 %. Also, if U is a speed characteristic of meso- and large-scale atmospheric systems, we have $U \ll$ speed of sound. Then to a reasonable approximation we may use as a lower boundary condition

$$w = 0 \quad \text{at} \quad z = 0.$$

It has recently been shown in one frontal study (Hoskins 1973) that the error thus introduced is indeed negligible.

2.2. *The geostrophic and quasi-geostrophic approximations*

Let L and U denote scales for horizontal distance and velocity, and suppose that $D/Dt \sim U/L$. Then the ratio of the acceleration terms to the Coriolis force terms is the Rossby number U/fL. For large-scale motions in the extratropical atmosphere of the earth this number is generally small. To a first approximation the Coriolis force balances the pressure force and the velocities are geostrophic:

$$u = -\phi_y/f, \quad v = \phi_x/f.$$

Combining these with the hydrostatic equation gives the so-called thermal-wind relations for the vertical shears in horizontal velocity:

$$fu_z = -g\theta_y/\theta_0, \quad fv_z = g\theta_x/\theta_0.$$

If the potential temperature decreases polewards, the westerly wind increases with height.

In the quasi-geostrophic approximation (see, for example, Pedlosky 1964), the expansion is carried to second order in Rossby number to obtain a predictive equation. In this approximation, the vertical component of vorticity calculated from the geostrophic velocities is advected by the geostrophic motion and changed only by stretching of the basic vorticity f by a vertical velocity. This vertical velocity is calculated from geostrophic advection of the temperature field, assuming a static stability dependent only on height.

An atmospheric front is a region in which the Rossby number is not small and the failure of quasi-geostrophic theory to produce realistic fronts is not surprising (Stone 1966; Williams & Plotkin 1968).

2.3. *The cross-front geostrophy approximation*

We now consider a frontal situation in which gradients in the x direction are much larger than those in the y direction. Let L_x, L_y, U and V denote length and velocity scales in the two horizontal directions. Taking U/L_x as a measure of D/Dt, the ratios of the accelerations to the Coriolis force terms in the two horizontal momentum equations are

$$\frac{U^2}{V^2}\frac{V}{fL_x}, \quad \frac{V}{fL_x}.$$

In such a frontal situation the latter number, a dimensionless measure of relative vorticity, may be of order one. But, relative to a front oriented in the y direction, it is found that $U \ll V$. To describe the production of a realistic front, the long-front acceleration may not be ignored. However, until the front becomes extremely strong, the cross-front acceleration may be neglected. This implies that the long-front wind is in geostrophic balance with the cross-front pressure gradient (see figure 1). We retain the thermal-wind balance

$$fv_z = (g/\theta_0)\,\theta_x.$$

The consistency of this approximation has been demonstrated in earlier studies.

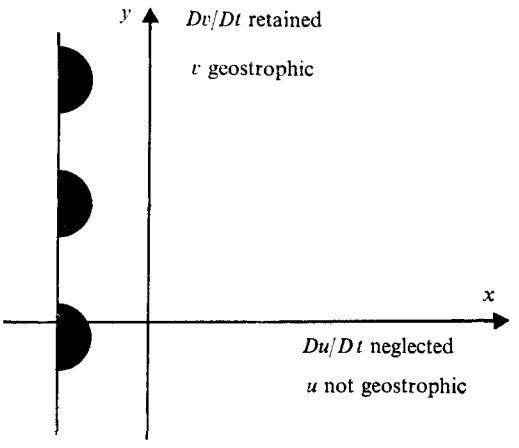

FIGURE 1. A schematic illustration of the cross-front geostrophy approximation. Using the usual meteorological symbolism, the scalloped line parallel to the y axis represents a front. The gradients perpendicular to this line are much larger than those parallel to it.

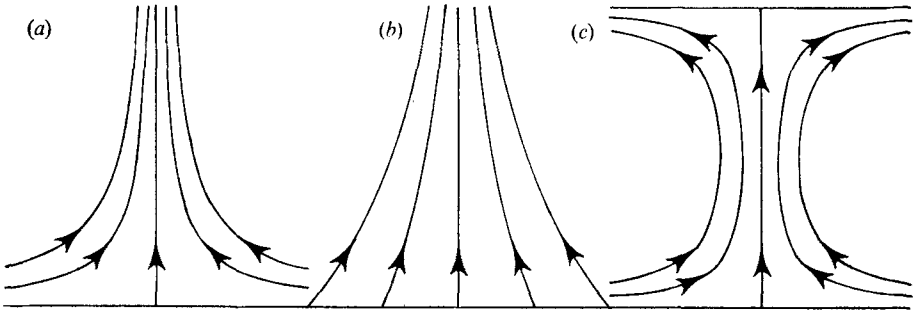

FIGURE 2. Basic horizontal velocity fields providing deformation.
(*a*) αxy. (*b*) $ax\,e^{by}$. (*c*) $ax \sin by$.

3. A deformation field

We first consider the advection of a passive scalar θ by a basic horizontal velocity field derived from a stream function

$$\psi_b = xA(y).$$

Then
$$u_b = -xAy, \quad v_b = A. \tag{3.1}$$

Insertion in (2.1) shows that this is a possible solution only if

$$A_y^2 - AA_{yy} = \text{constant} = \alpha^2, \quad \text{say}, \tag{3.2}$$

and then
$$\phi_b = fxA - \tfrac{1}{2}A^2 - \tfrac{1}{2}\alpha^2 x^2.$$

The solutions of (3.2) are of the form

$$\alpha y, \quad a\,e^{by} \quad (\alpha = 0), \quad a \sin by \quad (\alpha = ab).$$

Streamlines of the three flows are shown in figure 2.

In a flow of this form, a line element initially parallel to the x axis remains so. If its length is L, then LA is constant following the element. The time-independent solution for the distribution of the passive scalar θ is

$$\theta = \Theta(\psi_b) = \Theta(xA).$$

Clearly the advection of potential temperature by the basic deformation field is not such a simple problem. The above solution should however be valid when the implied gradients of potential temperature are small enough in some sense, e.g. for sufficiently small y in the fields in figures 2(*a*) and (*c*). When the implied gradients are large we expect that nonlinear distortions similar to atmospheric frontogenesis should occur. We shall consider situations in which temperature variations are negligible except in some region near $x = 0$. Thus, for large x, we may assume passive advection.

4. Analysis of the time-independent model

4.1. *General*

The equations of motion (2.1) in general describe the conservation moving with fluid particles of the following two properties.

(i) Potential temperature θ (conservation of entropy).

(ii) Ertel's potential vorticity $q = r^{-1}(f\mathbf{k} + \nabla \times \mathbf{u}) . \nabla\theta$.

In steady motion, Bernoulli's theorem gives a third conserved property. This property, which we shall call the Bernoulli function, is

(iii) $B = \phi + \frac{1}{2}(u^2 + v^2) + c_p T$.

The first term is the potential energy. The second term is the kinetic energy and the third the enthalpy (internal energy plus p/ρ). Since the hydrostatic relation is

$$\theta = \theta_0 \phi_z / g$$

and the co-ordinate z is such that

$$c_p T = (c_p - gz/\theta_0)\,\theta,$$

the three conserved properties may be written in terms of position, ϕ, u and v:

$$\begin{aligned} &\text{(i)} \quad g\theta/\theta_0 = \phi_z, \\ &\text{(ii)} \quad gq/\theta_0 = r^{-1}[-v_z\phi_{xz} + u_z\phi_{yz} + (f + v_x - u_y)\,\phi_{zz}], \\ &\text{(iii)} \quad B = \phi + \tfrac{1}{2}(u^2 + v^2) - z\phi_z + k(\phi_z), \end{aligned}$$

where k is an arbitrary function.

4.2. *Cross-front geostrophic analysis*

Without loss of generality, in (2.1) we set u, v and ϕ equal to their deformation-field values plus extra terms,

$$u = -xA_y + u', \quad v = A + v', \quad \phi = \phi_b + \phi',$$

and obtain for the horizontal momentum equations

$$\left.\begin{aligned} Du'/Dt - A_y u' - xA_{yy}v' - fv' + \phi'_x = 0, \\ Dv'/Dt + A_y v' + fu' + \phi'_y = 0. \end{aligned}\right\} \tag{4.1}$$

The cross-front geostrophy approximation here is to neglect the first three terms in (4.1) and set $v' = v'_g$, where $$fv'_g = \phi'_x.$$

Clearly this is valid only for $|x| \ll |f/A_{yy}|$. Under this approximation, the three conserved quantities may be written in terms of position and ϕ' only:

(i) $g\theta/\theta_0 = \phi'_z$,

(ii) $fgq/\theta_0 = r^{-1}[-\phi'^2_{xz} + (f^2 + \phi'_{xx})\phi'_{zz}]$,

(iii) $B = \phi_b + \phi' + \frac{1}{2}(A + \phi'_x/f)^2 + \frac{1}{2}\alpha^2 x^2 - z\phi'_z + k(\phi'_z)$.

Under the cross-front geostrophic assumption, the cross-front velocity disappears from these relations.

If the state of the fluid is known at one value of y (y_I, say) and the flow is downstream then the three Lagrangian markers, entropy, potential vorticity and the Bernoulli function, enable a solution to be obtained. From the section at y_I, q is known as a function of B and θ in the interior of the fluid, and θ is known as a function of B on horizontal boundaries. A numerical solution using iteration is, in principle, possible.

4.3. *The geostrophic co-ordinate*

As described in detail in II, in order to make analytical progess in the previous studies of nonlinear frontogenesis, it was necessary to introduce a new independent variable in the x direction: $$X = x + v'_g/f.$$

Instead of ϕ', a new dependent variable

$$\Phi' = \phi' + \tfrac{1}{2}v'^2_g$$

was also considered. In the problem considered here, a solution could be obtained without a co-ordinate transformation. However, the conserved quantities and hence the solution by numerical techniques are simplified if the transformation is made.

The Jacobian of the transformation to X space is the non-dimensional vertical component of absolute vorticity under the cross-front geostrophy approximation:

$$\zeta/f = 1 + v'_{gx}/f = [1 - v'_{gX}/f]^{-1}.$$

It is convenient to introduce Y, Z, and T to denote y, z and t when using X as the independent variable in the x direction. It may be shown that the three-dimensional gradient of Φ in X space is identically equal to that of ϕ' in x space. In particular, $$fv'_g = \Phi_X, \quad g\theta/\theta_0 = \Phi_Z.$$

Further, it may be shown that $$q = r^{-1}\zeta\theta_Z.$$

It may then be verified that the conserved quantities can be written more simply in terms of position and Φ:

(i) $g\theta/\theta_0 = \Phi_Z$,

(ii) $$gq/(f\theta_0) = \frac{1}{r}\frac{\Phi_{ZZ}}{1 - \Phi_{XX}/f^2},$$

(iii) $B = fXA + \Phi - Z\Phi_Z + k(\Phi_Z)$.

The state of the fluid at $Y = Y_I$, say, determines the functions $q(\theta, B)$ in the interior and $\theta(B)$ on horizontal boundaries. Then, at any Y,

$$\frac{1}{f^2}\Phi_{XX} + \frac{f\theta_0}{gr(Z)}\frac{1}{q(\theta, B)}\Phi_{ZZ} = 1, \tag{4.2}$$

with $\theta = \theta(B)$ on horizontal boundaries. Thus the problem may be solved numerically by iteration.

The use of X simplifies the constraints, and it is a stretched co-ordinate for regions of large vorticity such as fronts. This again makes numerical solution much easier. Since the approach to a discontinuity is just given by $\Phi_{XX}/f^2 \to 1$ ($\zeta \to \infty$), it is suggested that the nonlinearity of the original equations contains a tendency to produce frontal discontinuities in a finite time. This process was described in II.

It should be noted that the solution at a particular value of Y depends on the basic deformation field only through the local basic velocity $A(Y)$. It does not depend on which of the three deformation fields is present, or on the rate of deformation. This is clearly associated with neglecting the acceleration in the x direction as was done in the cross-front geostrophy approximation. Thus the solutions at particular cross-sections shown below are independent of the details of the deformation field and depend only on the deformation having taken place. Since the explicit X dependence is only linear in B, these solutions are also independent of the position of the axis of the basic deformation field ($x = 0$) with respect to the temperature field.

The Jacobian of the transformation to (B, θ) co-ordinates from (X, Z) co-ordinates is

$$fv\theta_Z = frvq/\zeta.$$

Thus the transformations to (X, Z) co-ordinates and then to (B, θ) co-ordinates are valid for a finite, positive vertical component of absolute vorticity, positive potential vorticity and no reversals in the progress downstream.

Finally, to aid the setting of initial conditions and side boundary conditions well away from the region of large temperature gradients, we note that the condition that there is zero total perturbation momentum in a fluid column is

$$\int_0^{Z_a} rv_g\, dZ = 0. \tag{4.3}$$

5. One-region model

5.1. *The model*

To find the functional relations between q, θ and B, we consider a cross-section at $Y = Y_I$ at which the temperature gradients are so weak that the vorticity of the associated winds is negligible compared with f, and θ is being advected as a passive scalar. In this one-region model we take the Brunt–Väisälä frequency N to be uniform at $Y = Y_I$, where

$$N^2 = \frac{g}{\theta}\frac{d\theta}{dh} = \frac{g}{\theta_0}\frac{d\theta}{dZ}.$$

Therefore
$$q = \theta_0 f N^2/[gr(Z_I)]$$

and
$$\theta(X_I, Z_I) = \theta_0 N^2 Z_I/g + \Theta_s(X_I/L_I),$$

where Θ_s is a known function with

$$[\Theta_s(X/L)]_{-\infty}^{\infty} = \Delta\theta, \quad \{d[\Theta_s(X/L)]/dX\}_{\max} = \Delta\theta/L.$$

Integration with respect to Z shows that we may take

$$\Phi(X_I, Z_I) = \tfrac{1}{2}N^2Z_I^2 + (Z_I - h)(g/\theta_0)\,\Theta_s(X_I/L_I) + gh.$$

h is chosen so that the zero-total-momentum condition (4.3) is satisfied. Taking

$$k = (g/\theta_0)\,h(\theta - \theta_0),$$

the Bernoulli function is

$$B(X_I, Z_I) = fX_IA_I + N^2Z_I(h - \tfrac{1}{2}Z_I).$$

Therefore, at $Z = 0$,
$$\theta(B) = \Theta_s(B/B_I), \tag{5.1}$$

where $B_I = fL_IA_I$, and at the upper horizontal boundary $Z = Z_T$, say,

$$\theta(B) = \frac{\theta_0 N^2}{g} Z_T + \Theta_s\left(\frac{B - N^2Z_T(h - \tfrac{1}{2}Z_T)}{B_I}\right). \tag{5.2}$$

Further,
$$q(B, \theta) = \theta_0 fN^2/[gr(Z_I)],$$

where $Z_I(B, \theta)$ is a solution of the transcendental equation

$$Z_I = \left[\theta - \Theta_s\left(\frac{H - N^2Z_I(h - \tfrac{1}{2}Z_I)}{B_I}\right)\right]\frac{g}{\theta_0 N^2}. \tag{5.3}$$

Since B_I is conserved in passive advection, the functional forms are independent of the choice $Y = Y_I$ provided that it is in the region of passive advection.

At any Y downstream, the solution may be obtained by solving (4.2), which here becomes

$$\frac{1}{f^2}\Phi_{XX} + \frac{1}{N^2}\frac{r(Z_I)}{r(Z)}\Phi_{ZZ} = 1, \tag{5.4}$$

with Z_I given by (5.3) and boundary values $(\theta_0/g)\,\Phi_Z$ given by (5.1) and (5.2), where

$$B = \underset{1}{fXA} + \underset{2}{(\Phi - gZ)} - \underset{3}{(g/\theta_0)\,(\theta - \theta_0)}\,(Z - h). \tag{5.5}$$

Since in this section we are interested in studying the formation of surface fronts and in the atmosphere the stability increases markedly above the tropopause, we place our upper boundary at $Z = H < Z_a$. The Boussinesq-type approximation of replacing $r(Z_I)/r(Z)$ by unity in (5.4) is also made, and its validity in one example will be checked. For the order-of-magnitude arguments below, we note that $h = O(\frac{1}{2}H)$.

5.2. *Dimensionless parameters and comparison with previous work*

An upper bound on the magnitude of the thermal wind v' at the surface may be obtained by assuming passive advection of the potential-temperature field. Comparison with the basic y velocity then gives the following condition that the flow should be downstream:

$$\beta = gh\Delta\theta/\theta_0 B_I < 1.$$

In the time deformation model only the case $\psi_b = \alpha xy$ was considered. If Φ was initially independent of Y, it remained so. The equations were identical with those above except that only the first term of (5.5) occurred in B. In this term, $A(Y)$, which is a measure of the deformation with distance downstream, was replaced by $e^{\alpha T}$, a measure of the deformation with time. When it is a good approximation to neglect the extra terms in B, then the solutions for downstream frontogenesis are the same as those for frontogenesis in time. There are two situations in which this should be valid.

(i) When the thermal wind is negligible compared with the basic velocity; then terms 2 and 3 in (5.5) are each negligible compared with term 1. This condition is $\beta \ll 1$.

(ii) When terms 2 and 3 tend to cancel each other. The Laplace equation (5.4) suggests that this is consistent if the length scale L of the temperature field on the boundaries is much larger than the 'Rossby radius of deformation' NH/f. But for frontogenesis to occur, the vorticity of the wind derived from the thermal-wind relation must be comparable with the Coriolis parameter:

$$\frac{1}{f}\frac{g}{\theta_0}\frac{\Delta\theta}{L^2}h \sim f.$$

Using this relation to estimate L, the condition becomes

$$\Delta_Z\theta \ll \Delta\theta,$$

where $\Delta_Z\theta = \theta_0 N^2 H/g$ is a measure of the vertical potential-temperature difference in the passive advection state.

The special case of zero potential vorticity ($N = 0, \Delta_Z\theta = 0$) solved analytically in II is an *exact* solution of the present problem also. The potential temperature is a function of X only and there is exact cancellation between terms 2 and 3 in B. The solutions exhibited previously showed the formation of surface fronts which were remarkably realistic considering the simplicity of the model.

5.3. *Numerical solutions*

The general method of solution is a numerical relaxation. For a fixed $A(Y)$, a finite region of the X, Z plane is covered by a uniform grid. The boundaries at constant X are chosen to be away from the region of temperature contrast so that on them passive advection is a good approximation. Taking as initial conditions that Φ has its passive-advection value everywhere gives values for B and Z_I everywhere, and hence θ on boundaries and q in the interior as a function of position. Using these values, we relax towards a solution of (5.4). After a number of iterations, new values of B are found from (5.5) and of Z_I from (5.3) in the form

$$Z_I^{n+1} = \theta - \Theta_s([B^n - N^2 Z_I^n(h - \tfrac{1}{2}Z_I^n)]/B_I),$$

where the superscript $n+1$ refers to the new value and n to the old value. Thus new values of θ on the boundaries and of q in the interior are found. The process is repeated until the required convergence is obtained. If the Boussinesq approximation is made, then the calculation of Z_I is omitted. When a solution for Φ in

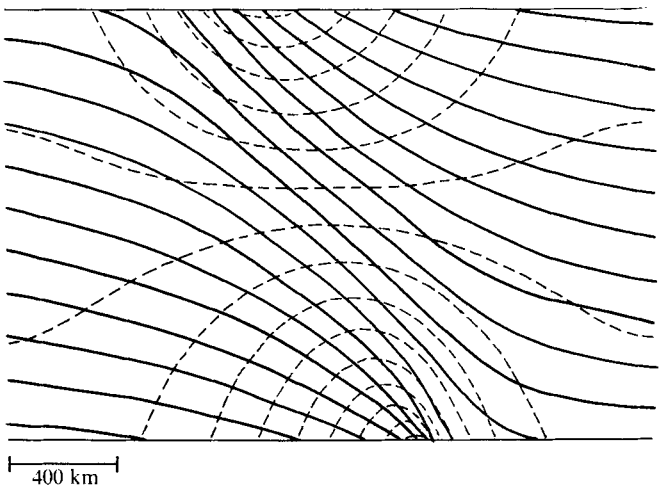

FIGURE 3. Solution at the cross-section of the one-region model at $A = 40\,\mathrm{ms}^{-1}$. – – –, contours of long-front velocity drawn every 4 ms^{-1}; ——, contours of potential temperature drawn every 2·4 °K.

X space has been obtained, v_g' and θ are obtained by horizontal and vertical differencing and the transformation to physical space performed:

$$x = X - v_g'/f.$$

We now consider an example in which neither of the conditions (i) and (ii) is met. We choose as in I

$$H = 8\,\mathrm{km} \sim 300\,\mathrm{mb}, \quad f = 10^{-4}\,\mathrm{s}^{-1}, \quad g/\theta_0 = \tfrac{1}{30}\,\mathrm{ms}^{-2}\,^\circ\mathrm{K}^{-1},$$

$$N = 10^{-2}\,\mathrm{s}^{-1}, \quad \Theta_s(X/L) = (\Delta\theta/\pi)\tan^{-1}(\pi X/L), \quad \Delta\theta = \Delta_Z\theta = 24\,^\circ\mathrm{K}.$$

There is cold air at $x = -\infty$ and warm air at $x = +\infty$. The thermal wind at the surface opposes the basic flow and that at the 'lid' reinforces it. We choose B_I so that $\beta = 0{\cdot}917$ and the surface thermal wind is only a little smaller than the basic wind.

The solution at the cross-section at $A = 40\,\mathrm{ms}^{-1}$ is shown in figure 3. Near the surface, the positive values of the vertical component of relative vorticity are larger than the negative values. The values of positive vorticity and temperature gradient are largest at the surface and fall off rapidly with height. At each level, gradients are a maximum in a region whose slope is approximately one in one hundred. This surface front is very similar to those described in the previous studies and compared there with atmospheric fronts. The maximum absolute vorticity at the surface is approximately $4f$. This value was attained in the previous models at a deformation equivalent to $A = 60\,\mathrm{ms}^{-1}$. In contrast, the frontogenesis at the rather unrealisitic lid is retarded compared with the time deformation model. The maximum absolute vorticity there is only $1{\cdot}5f$.

In figure 4 are exhibited the Lagrangian co-ordinates B and θ, together with the (x, z) motions of some fluid particles from their position at $A = 32\,\mathrm{ms}^{-1}$. At that cross-section, the maximum absolute vorticity was approximately $2f$.

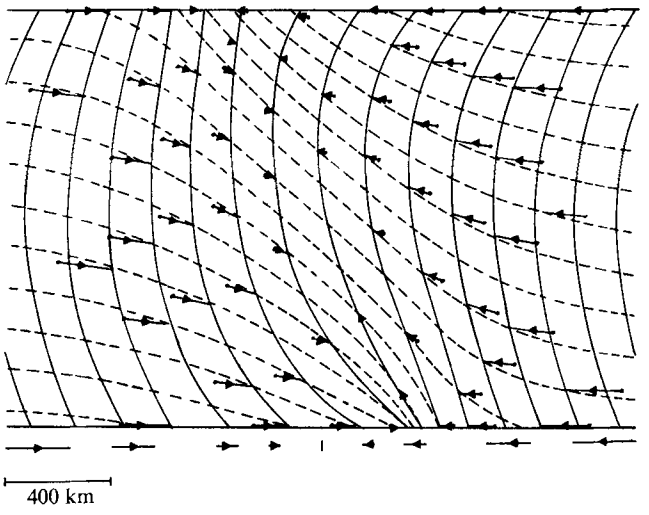

FIGURE 4. Contours of the Bernoulli function (solid lines) and potential temperature (dashed lines) at $A = 40\ \mathrm{ms}^{-1}$, together with the cross-front motion of some fluid particles from $A = 32\ \mathrm{ms}^{-1}$. The motion implied by the basic deformation field alone is shown beneath the lower surface.

Comparison with the basic deformation shown beneath indicates the enhanced convergence at the surface front and strong upward motion. The up-gliding of the warm air and down-gliding of the cold air are also evident. If the deformation occurs in the first basic stream function with $\alpha = 10^{-5}\mathrm{s}^{-1}$, then the distance between the cross-sections is 800 km. Air near the surface front takes approximately one day to travel this distance. The near coincidence of the B and θ lines in the region of the surface front indicates the small value of the Jacobian of the transformation there.

Solving the problem for various values of A, and using the same basic deformation field, yields the description of the motion of fluid particles at the surface given in figure 5. Again the strong convergence at the surface front is evident.

Also, this model predicts infinite vorticity and the formation of frontal discontinuities at a finite basic deformation ($A \sim 45\ \mathrm{ms}^{-1}$). This will be commented on below.

This problem for $A = 40\ \mathrm{ms}^{-1}$ was solved also without making the Boussinesq approximation. The ratio $r(Z_I)/r(Z)$ varied smoothly between 0·94 and 1·07 and the solution differed little, confirming the validity of the Boussinesq approximation in the surface frontogenesis model.

If we now consider the problem with the warm air at $x = -\infty$ and cold air at $x = +\infty$, the thermal wind opposes the basic flow at the lid and reinforces it at the surface. As may be anticipated, the surface frontogenesis is retarded compared with the time deformation solution. The lid frontogenesis is increased.

The final one-layer model to be discussed is as above but with $\Delta\theta = 6\ ^\circ\mathrm{K}$. Then $\beta = 0{\cdot}229$, so that the thermal wind is expected to be much smaller than the basic wind. Unrealistically large values of A are required to obtain real frontogenesis. With the thermal wind opposing the basic flow at the surface, and

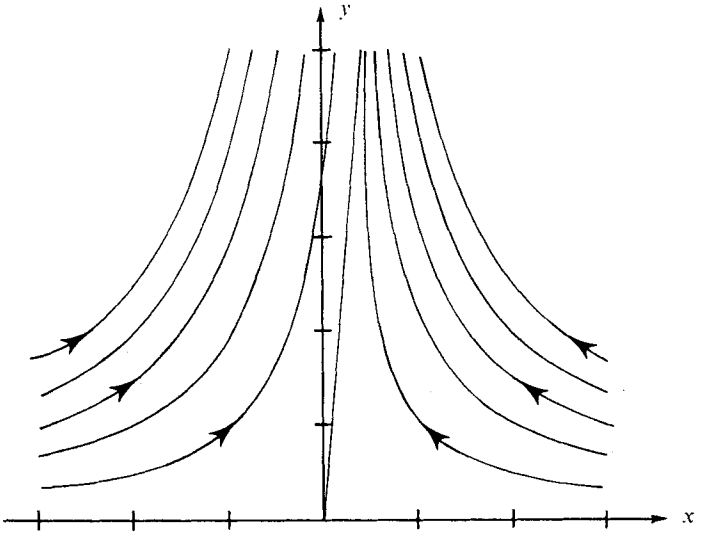

FIGURE 5. Streamlines at the surface taking $\psi_b = \alpha xy$. The tick marks indicate spacings of 800 km on the axes.

$A = 160\,\mathrm{ms}^{-1}$, the maximum values of the absolute vorticity at the surface and lid are $2{\cdot}2f$ and $1{\cdot}8f$ respectively. The smallness of the asymmetry between the surface and lid is in agreement with the condition (i) for negligible difference from the time deformation solution

6. Two-region model

6.1. *The model*

To describe the formation of upper tropospheric fronts, we consider a model with two regions of uniform stability. The large-stability region above (region 2) represents the stratosphere and the low-stability region below (region 1) represents the troposphere. The surface of discontinuity between the two regions models the tropopause. Given the initial conditions at $Y = Y_I$, the potential temperature θ is known as a function of the Bernoulli function B on the surface, the tropopause and the lid. The ratio $\mu = r(Z_I)/r(Z)$ is known as a function of θ, B and Z. The velocity is continuous across the tropopause, and so Φ must be continuous across this boundary, whose position is unknown. In the two regions we have

$$\frac{1}{f^2}\Phi_{1XX}+\frac{\mu}{N_1^2}\Phi_{1ZZ} = 1, \quad \frac{1}{f^2}\Phi_{2XX}+\frac{\mu}{N_2^2}\Phi_{2ZZ} = 1.$$

The problem is thus a closed one.

In the solutions described here, the initial slope of the tropopause is such that the potential-temperature gradient at the lid is zero and no frontogenesis will occur there. Thus, at $Y = Y_I$, the height h_t of the tropopause is a function of the surface temperature Θ_s. In a manner similar to the one-layer model, we take

$$\Phi = \begin{cases} \frac{1}{2}N_1^2Z_I^2+(Z_I-h)(g/\theta_0)\Theta_s(X_I/L_I)+gh & (Z_I < h_t), \\ \frac{1}{2}N_1^2Z_I^2+(Z_I-h)(g/\theta_0)\Theta_s(X_I/L_I)+gh+\frac{1}{2}(N_2^2-N_1^2)(Z_I-h_t)^2 & (Z_I > h_t). \end{cases}$$

Since h_t is a function of Θ_s, the zero-total-momentum condition implies that h is a slowly varying function of Θ_s. To an extremely good approximation, this variation is linear:

$$h = h_0 + \epsilon\Theta_s.$$

In the solutions exhibited here this variation is included though its effect has been found to be negligible. As before, we choose

$$k = (g/\theta_0)\, h_0(\theta - \theta_0),$$

and then the Bernoulli function is

$$B(X_I, Z_I) = fX_I A_I + N_1^2 Z_I(h_0 - \tfrac{1}{2}Z_I) - \epsilon\Theta_s.$$

In the upper layer, since the lid temperature Θ_l is uniform, the Bernoulli function is not required. The ratio μ is known as a function of θ and Z since

$$Z_I = H - (\Theta_l - \theta)\, g/(\theta_0 N_2^2).$$

6.2. *The numerical scheme*

The problem is solved by relaxation as in III and § 5.3. The major difficulty is that the position of the internal boundary is unknown. It is fixed and 15 iterations performed, demanding only continuity of Φ and θ across it. New values of the Bernoulli function, and thus of the correct potential temperature, on it are then calculated. Comparing these with the actual values in the vicinity, the tropopause is moved such that the values of potential temperature on it are likely to be nearer the correct ones.

6.3. *Three solutions*

The initial temperature distribution and the values of constants used for the solutions below are as in experiment 4 in I and in III. There is a large surface potential-temperature contrast of 49 °K and a weak minimum in potential temperature on the cold side of the transition zone. The compensating initial tropopause is at 293 mb on the cold side, descends to 304 mb at the minimum in potential temperature and rises to 200 mb on the warm side. The constants used are

$$N_1 = 10^{-2}\,\mathrm{s}^{-1}, \quad N_2 = 3\times 10^{-2}\,\mathrm{s}^{-1}, \quad f = 10^{-4}\,\mathrm{s}^{-1},$$

$$\theta_0/g = 30\,\mathrm{m}^{-1}\mathrm{s}^2\,^\circ\mathrm{K}, \quad R = 287\,\mathrm{m}^2\mathrm{s}^{-2}\,^\circ\mathrm{K}^{-1}, \quad H = 13{\cdot}1\,\mathrm{km} \quad \text{(lid at 135 mb)}.$$

(i) The first solution is for a case in which B_I is chosen such that the thermal wind near the tropopause reinforces the basic flow and that at the ground opposes the basic flow but is not as large. In figure 6 is exhibited the solution for the large value $A = 157\,\mathrm{ms}^{-1}$, which with the B_I chosen implies a basic deformation equivalent to the NB 6 model of III. A frontal discontinuity has formed at the surface. The maximum surface thermal wind ($63\,\mathrm{ms}^{-1}$) is, indeed, not comparable with the basic wind. Comparing the tropopause with its passive-scalar shape shown above, we note the descent of a tongue of stratospheric air and the formation of strong gradients in the region of the tongue. This is very similar to NB 6 though the development has not proceeded as far. The maximum descent is

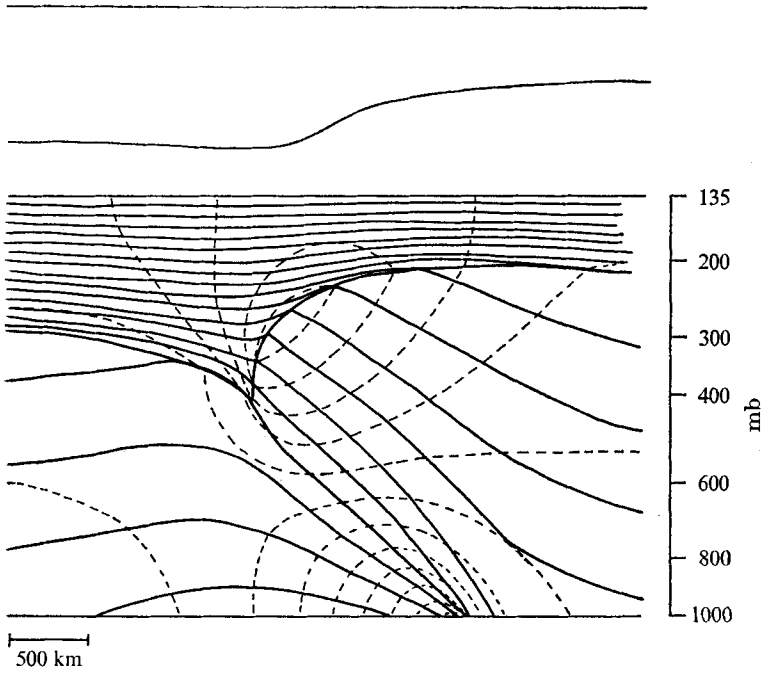

FIGURE 6. Solution at the cross-section of the two-region model (i) at $A = 157\ \mathrm{ms}^{-1}$. – – –, contours of long-front velocity drawn every $10{\cdot}5\ \mathrm{ms}^{-1}$; ——, contours of potential temperature drawn every 7·8 °K. Above is shown the shape the tropopause would have had if the fluid had contracted passively under the basic deformation field.

111 mb compared with 128 mb and the maximum absolute vorticity at the tropopause $3{\cdot}7f$ compared with $4{\cdot}6f$.

To show the cross-front motions involved in the development, figure 7 exhibits some fluid particle motions from the cross-section at $A = 118\ \mathrm{ms}^{-1}$. There the maximum descent is 74 mb and the maximum absolute vorticity $2{\cdot}7f$. These cross-front motions are qualitatively identical to the schematic picture presented by Danielsen (1968), synthesized from his synoptic studies.

(ii) The second solution is for the same case as the first except that B_I is two-thirds of the value used there. We show in figure 8 the solution at the cross-section at $A = 79\ \mathrm{ms}^{-1}$, at which the deformation by the basic field is the same as at $A = 118\ \mathrm{ms}^{-1}$ in (i). The maximum thermal wind at the surface is $77\ \mathrm{ms}^{-1}$, so that the downstream condition is only just valid there. A frontal discontinuity has formed at the surface. The development of the upper troposphere is much smaller than in (i), with a maximum descent of 68 mb and a maximum absolute vorticity $2{\cdot}3f$.

(iii) The third solution is for the same case as the second except that the temperature contrast is reversed so that the thermal wind opposes the basic wind at the tropopause, and reinforces it at the surface. The solution at the cross-section at $A = 79\ \mathrm{ms}^{-1}$ is shown in figure 9. The maximum tropopause descent is 101 mb and the maximum absolute vorticity $4{\cdot}0f$. There is a sharp change in

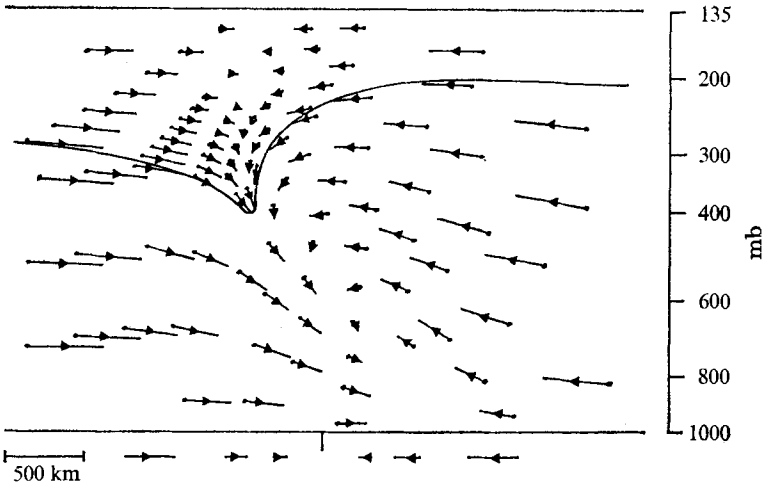

FIGURE 7. Two-region model (i). Cross-front motions from $A = 118$ ms^{-1} to $A = 157$ m
The basic deformation motion is shown below the lower surface.

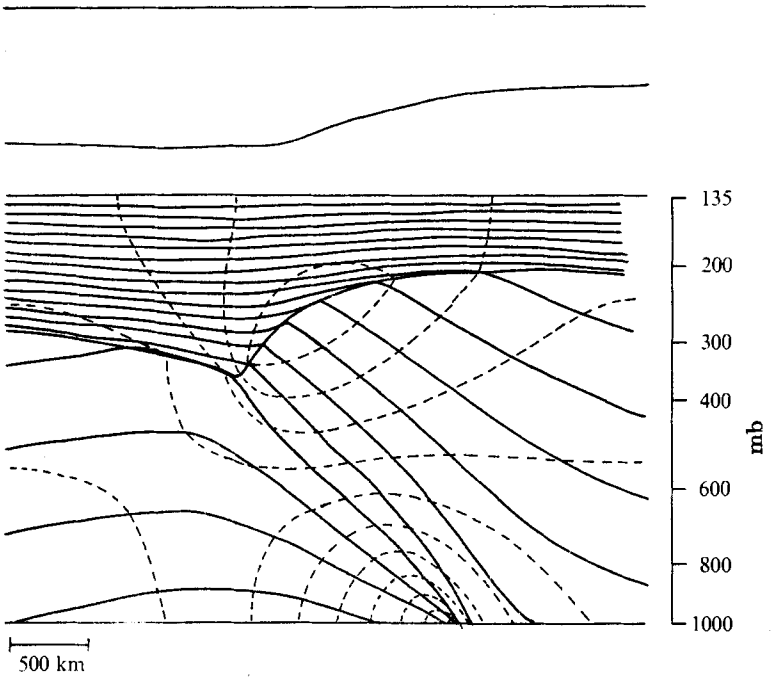

FIGURE 8. Two-region model (ii) at $A = 79$ ms^{-1}. Notation as in figure 6.

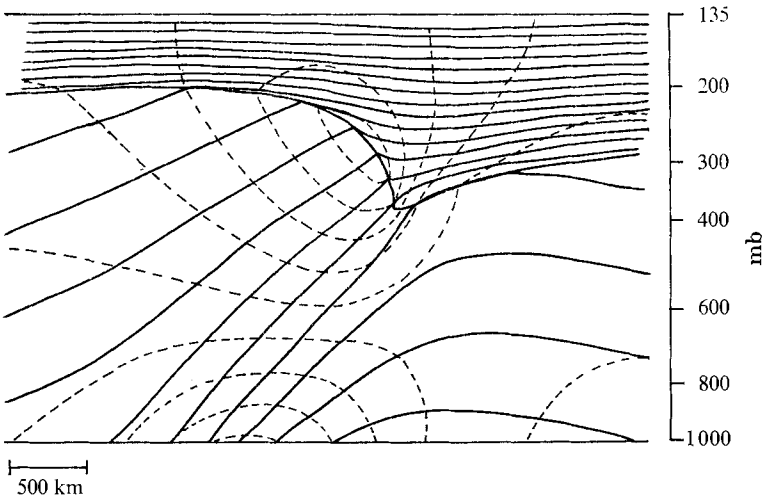

FIGURE 9. Two-region model (iii) at $A = 79$ ms^{-1}. Notation as in figure 6. The 'undisturbed' tropopause shape would be the reflexion of that shown in figure 8.

tropopause slope, which even in X co-ordinates means that the relaxation procedure has to be performed carefully. The surface front has not developed at this stage.

7. Discussion

The above solutions do not differ greatly from those found previously using the time deformation model. In that problem, the frontogenesis was not dependent on the direction of the thermal wind. However, the solutions given here for the downstream frontogenesis model suggest that, in this model, the frontogenesis can be modified. The conditions for this to occur are that the thermal wind is comparable with the basic wind, and the vertical potential-temperature difference through the depth of the troposphere is of the same order as the temperature difference across the baroclinic zone. The nonlinear frontogenesis described is increased where the thermal wind opposes the basic deformation field and decreased where it reinforces it. This may be understood by considering (5.5) with variables represented by perturbations from standard values at that level:

$$\theta = \theta_0 + N^2\theta_0 Z/g + \theta', \quad \Phi = gZ + \tfrac{1}{2}N^2Z^2 + \Phi'.$$

Then, at $Z = 0$,
$$B_X = fA + \frac{g}{\theta_0}\left(h\theta'_X - \int_0^h \theta'_X\, dZ\right) + \Phi'|_{Z=h}. \tag{7.1}$$

But the condition $\Delta_Z\theta \sim \Delta\theta$ implies (see §5.3) that the interior potential-temperature distribution is modified owing to the necessity for conservation of potential vorticity. The modification is such as to produce weaker temperature gradients. Therefore

$$|h\theta'_X| \geqslant \left|\int_0^h \theta'_X\, dZ\right|$$

and both have the same sign. Neglecting the last term in (7.1), this implies that for A positive the cross-front gradient of B is increased for positive gradients of potential temperature and decreased for negative ones. A similar argument shows that at the tropopause the cross-front gradient of B is increased or decreased according as the potential-temperature gradient is negative or positive.

The approximation of cross-front geostrophic balance will no longer be valid where the fronts described in this paper become extremely strong. We may consider that the frontogenesis is occurring in a field of type (iii) such that the maximum frontal gradients are small enough for the approximation to be valid. The solution downstream from that point is identical to that upstream as the cross-front accelerations have been neglected. Alternatively, as described in the earlier papers, we may estimate the stage at which cross-front accelerations become important. Assuming reasonable values for the deformation fields, it is found that the real restriction on these models is the neglect of mixing effects. Since in a strong front the Richardson number $\sim f/\zeta$, these effects must be important by the time that the absolute vorticity is $5f$. However, we may say that there is a tendency for discontinuities to form at surface fronts, and for sharp upper-air fronts to form, with only a finite externally imposed deformation.

This work was performed when the author was in the Advanced Study Program of the National Center for Atmospheric Research. Much of the background originated in discussions with Dr Francis Bretherton. Thanks are also due to Dr Stephen Fels for suggesting clarifications in the manuscript. Support was provided through the Geophysical Fluid Dynamics Laboratory/NOAA Grant E22-21-70(G).

REFERENCES

BJERKNES, J. 1919 On the structure of moving cyclones. *Geofys. Publikasjoner*, **1**, 1–8.

CHARNEY, J. G. 1947 The dynamics of long waves in a baroclinic westerly current. *J. Meteor.* **4**, 135–162.

DANIELSEN, E. F. 1968 Stratospheric–tropospheric exchange based on radioactivity, ozone and potential vorticity. *J. Atmos. Sci.* **25**, 502–518.

EADY, E. T. 1949 Long waves and cyclone waves. *Tellus*, **1**, 33–52.

HOSKINS, B. J. 1971 Atmospheric frontogenesis: some solutions. *Quart. J. Roy. Met. Soc.* **97**, 139–153.

HOSKINS, B. J. 1972 Non-Boussinesq effects and further development in a model of upper tropospheric frontogenesis. *Quart. J. Roy. Met. Soc.* **98**, 532–541.

HOSKINS, B. J. 1973 The surface pressure distribution in a simple frontogenesis model. *U.K. Universities Atmos. Modelling Group Rep.*

HOSKINS, B. J. & BRETHERTON, F. P. 1972 Atmospheric frontogenesis models: mathematical formulation and solution. *J. Atmos. Sci.* **29**, 11–37.

PEDLOSKY, J. 1964 The stability of currents in the atmosphere and ocean: Part I. *J. Atmos. Sci.* **21**, 201–219.

REED, R. J. & DANIELSEN, E. F. 1959 Fronts in the vicinity of the tropopause. *Arch. Meteor. Geophys. Bioklim.* A **11**, 1–17.

SANDERS, F. 1955 Investigation of the structure and dynamics of an intense surface frontal zone. *J. Meteor.* **12**, 542–552.

STONE, P. H. 1966 Frontogenesis by horizontal wind deformation fields. *J. Atmos. Sci.* **23**, 455–465.

WILLIAMS, R. T. & PLOTKIN, J. 1968 Quasi-geostrophic frontogenesis. *J. Atmos. Sci.* **25**, 201–206.